Lab on a Chip

RSC Publishing

PAPER

View Article Online
View Journal | View Issue

A Microfluidic Platform for Evaporation-based Salt Screening of Pharmaceutical Parent compounds†

Cite this: *Lab Chip*, 2013, **13**, 1708

Sachit Goyal,[a] Michael R. Thorson,[a] Cassandra L. Schneider,[a] Geoff G. Z. Zhang,[b] Yuchuan Gong*[b] and Paul J. A. Kenis*[a]

We describe a microfluidic platform to screen for salt forms of pharmaceutical compounds (PCs) *via* controlled evaporation. The platform enables on-chip combinatorial mixing of PC and salt former solutions in a 24-well array (~200 nL/well), which is a drastic reduction in the amount of PC needed per condition screened compared to traditional screening approaches that require ~100 μL/well. The reduced sample needs enable salt screening at a much earlier stage in the drug development process, when only limited quantities of PCs are available. Compatibility with (i) solvents commonly used in the pharmaceutical industry, and (ii) Raman spectroscopy for solid form identification was ensured by using a hybrid microfluidic platform. A thin layer of elastomeric PDMS was utilized to retain pneumatic valving capabilities. This layer is sandwiched between layers of cyclic-olefin copolymer, a material with low air and solvent permeability and low Raman background to yield a physically rigid and Raman compatible chip. A solvent-impermeable thiolene layer patterned with evaporation channels permits control over the rate of solvent evaporation. Control over the rate of solvent evaporation (2–15 nL h^{-1}) results in consistent, known rates of increase in the supersaturation levels attained on-chip, and increases the probability for crystalline solids to form. The modular nature of the platform enables on-chip Raman and birefringence analysis of the solid forms. Model compounds, tamoxifen and ephedrine, were used to validate the platform's ability to screen for salts. On-chip Raman analysis helped to identify six different salts each of tamoxifen and ephedrine.

Received 18th November 2012,
Accepted 21st February 2013

DOI: 10.1039/c3lc41271g

www.rsc.org/loc

Introduction

The pharmaceutical industry spends significant effort in finding solid forms of pharmaceutical parent compounds (PC) with desired physicochemical properties.[1–4] Salts, cocrystals, hydrates, solvates, and polymorphs are among the most commonly studied solid forms in the industry.[1,3–6] A certain solid form is typically selected for further development based on its favorable physicochemical properties, such as packing properties (*e.g.*, molar volume, hygroscopicity), thermodynamic properties (*e.g.*, melting point, entropy, enthalpy, solubility, vapor pressure, free energy), kinetic properties (*e.g.*, dissolution rate, reaction rates, stability), surface properties (*e.g.*, surface free energy, crystal habit), and mechanical properties (*e.g.*, hardness, tableting, flow ability).[1,4,6–10]

Methods such as solution crystallization, including reactive crystallization, antisolvent crystallization, slurry crystallization, temperature-controlled crystallization, vapor diffusion, and evaporative crystallization, are most commonly used to discover solid forms of PCs.[1,6] Other crystallization methods that have been reported to generate various solid forms include sublimation, thermal aging, grinding, melt crystallization, desolvation,[1,6] mechanochemistry,[11] laser-induced nucleation,[12] capillary crystallization,[13] and sono-crystallization.[14] Solution crystallization is usually preferred because of its scalability compared to other solid phase crystallization techniques, and its ability to immediately screen for hydrates and solvates, solid forms that incorporate solvent molecules.[6,15]

Preparation of salts of PCs *via* solvent evaporation allows for the generation of higher levels of supersaturation, thereby guaranteeing a phase transition to gels, precipitates, microcrystals, or crystals.[16,17] Nucleation takes time and usually occurs only above a certain supersaturation level. Traditional evaporative crystallization approaches, manual or automated, typically allow only limited control over the evaporation rate. If supersaturation levels increase too rapidly, insufficient time for nucleation will hamper the formation of crystalline solids.[16] Instead, amorphous precipitation or gel formation

[a]*Department of Chemical & Biomolecular Engineering, University of Illinois at Urbana-Champaign, 600 South Mathews Avenue, Urbana, Illinois 61801, USA. E-mail: kenis@illinois.edu; Tel: +1 (217) 265-0523*
[b]*Formulation Science, Global Pharmaceutical R & D, AbbVie Inc., 1 N Waukegan Road, North Chicago, Illinois 60064, USA. E-mail: yuchuan.gong@abbvie.com; Tel: +1 (847) 938-6642*

† Electronic supplementary information (ESI) available. See DOI: 10.1039/c3lc41271g

occurs. In prior work, we have reported platforms that allow crystallization of active pharmaceutical ingredients and proteins in aqueous solutions at the microliter scale by controlled evaporation method.[17–20] Our work as well as work by other has shown that precise control over the rate of solvent evaporation allows the system to remain at desired supersaturation levels for a sufficient amount of time to allow for nucleation to occur, thereby enhancing the probability for crystalline solids to form.[16–20]

Solution based salt screening of PCs is influenced by many factors, including supersaturation levels, the rate of change of supersaturation levels, the type of solvent and salt formers (SF), the PC and SF concentrations, pH, and temperature.[1,9,10,21] Numerous crystallization trials need to be conducted at various conditions to enhance the chance of identifying crystalline salts of the PC. These screens are performed either manually or with automated approaches that speed up the screening process and reduce the amount of PC consumed per condition tested.[1,4,7,22,23] However, these automated methods still require grams of PC to carry out a screen of 100 conditions in 100–500 μL wells[4] (at concentrations of 10–100 mg mL^{-1}). This sample requirement prevents solid form screening at the early stage of drug development when only small amounts of PC are available.[1,4,7] Consequently, salt screening is relegated to the later stages in drug development. Methods that would allow for salt screening with reduced sample needs per condition would allow for the identification of solid forms with desired physicochemical properties at an earlier stage. This in turn would significantly reduce the cost of drug development because costly switching to different solid forms at a later stage can be avoided.[4,23] Therefore, a screening method that requires at least one order of magnitude smaller quantities of PC is desired.[4,9,23]

Progress in microfluidics has led to the development of very-large scale integrated microfluidic platforms that allow precise control over on-chip metering of solutions, combinatorial mixing of very small sample volumes, and on-chip detection and analysis of chemical compounds, for example for screening applications.[24–29] Specifically, microfluidic approaches based on free interface diffusion (FID),[25,27,30] droplets,[31–35] solvent evaporation,[16,17,36] crystallization on engineered templates,[37] and slip-chip approaches[38] have been developed. These platforms have been employed to crystallize proteins and solid forms of PCs at the sub-μL to pL scale,[25,27,30–32,34,39–44] to study their solubility and phase diagrams,[18,39,45,46] and to study their crystallization kinetics.[19,32,47–50] However, most of the microfluidic crystallization tools reported to date suffer from one or more of the following limitations: (1) the materials used to fabricate the microfluidic chips are often incompatible with organic solvents commonly used in PC solid form screening,[51] and (2) the platforms are not amenable to on-chip solid form analysis. Typically, manual harvesting of crystals is needed for analysis using X-ray diffraction, Raman spectroscopy, solid state NMR, and/or IR spectroscopy (FTIR, near IR). Some of the reported microfluidic tools are compatible with one of the aforementioned analytical techniques and mild organics solvents[34,35] however, they have been limited to simple, single layer chip designs, which do not take advantage of the high-throughput, precise fluid handling capabilities of multilayer microfluidics. Droplet- and slip-chip based microfluidic tools[31,38,47] have enabled high-throughput screening of crystallization conditions but for example the PDMS-based droplet-based tools[47] lack the compatibility with organic solvents and slip-chip based tools[38] do not allow on-chip solid form analysis. Recently, we reported on microfluidic platforms for FID based solid form screening of PCs.[27,30,52] These platforms were compatible with water, alcohols, acetonitrile, and dimethylsulfoxide (DMSO), and allowed on-chip solid form analysis *via* Raman spectroscopy.[27,30,52] However, these platforms were not suitable for salt screening of PCs *via* solvent evaporation. To our knowledge, platforms capable of performing salt screening *via* evaporation at the sub-microliter scale have not been reported to date.

Here, we report on an evaporation-based microfluidic platform for salt screening of PCs that enables crystallization from initially under-saturated PC solutions. This microfluidic platform (1) requires less than 240 μg PC to screen for salts in 24 conditions, so less than 10 microgram of PC is needed per condition; (2) is compatible with solvents that are often used in pharmaceutical crystallization, *i.e.* water, alcohols; (3) permits better control over the rate of solvent evaporation (in the range of 2–15 nL h^{-1}) compared to current open-well techniques, thereby allowing consistent control over supersaturation; and (4) allows for on-chip Raman and birefringence analysis of the solid forms. We validated the platform by screening for salts of ephedrine and tamoxifen, resulting in the identification of six different salts of each model compound.

Materials and methods

Chip assembly

The crystallization platform consists a three-layer assembly (TLA, 200 μm thick) containing the fluid metering and mixing, an interfacial layer (IL, 60 μm thick), and an evaporation layer (EL, 2 mm thick) containing the channels that determine solvent evaporation rates. First the EL is fabricated (*vide infra*) and reversibly bonded with the IL. Then the EL-IL assembly is reversibly bonded to the TLA.

a. Three-layer assembly (TLA) fabrication. The TLA, comprised of the polydimethylsiloxane (PDMS, General Electric RTV 615, Part A/B) fluid layer (FL), the PDMS control layer (CL), and the cyclic olefin copolymer (COC, 6013 grade, TOPAS™ Advanced Polymers) backing layer were fabricated following the procedure reported previously.[52] As shown in Fig. 2a, control layers (80 μm) and fluid layers (70 μm) were prepared by spin coating 5 : 1 A : B, PDMS and 15 : 1 A : B, PDMS at 1100 and 1200 rpm, respectively, onto silicon wafers (University wafer) patterned with a negative photoresist Su-8 2050 (MicroChem) and thermally cured on a hot plate (Dataplate® 730 series, Barnstead Thermolyne). The COC-CL

was assembled by irreversibly bonding a 2 mil (50 μm) COC sheet to the top of the control layer after treatment with oxygen plasma in plasma cleaner for 1 min (Harrick Plasma). Holes were drilled (Dremel 300 series drill with a 750 μm McMaster-Carr drill bit) at the inlets of the control lines in the COC-CL, and then the assembly was manually aligned on to the FL. The TLA was lifted off and holes were drilled at the FL inlets and outlets. Next, a 3 mm thick PDMS block was irreversibly bonded to the top of the FL, followed by punching of through holes into the thick layer. See the ESI† for more details on the fabrication procedures.

b. Interfacial layer (IL) fabrication. A thin layer (10 μm) of PDMS (5 : 1 A/B) was spin coated at 5000 rpm on a blank silicon wafer pre-coated with a monolayer of tridecafluoro-1,1,2,2-tetrahydrooctyltrichlorosilane (Gelest). The thin layer of PDMS was then cured on a digital hot plate/stirrer (Dataplate® 730 series, Barnstead Thermolyne) at 80 °C for approximately 10 min. A 2 mil (50 μm) COC sheet was bonded irreversibly to the top of the PDMS layer *via* plasma bonding as shown in Fig. 2b. Then, the COC-thin layer assembly was heated at 80 °C for 10 min on a hot plate, after which it was carefully lifted off the silicon wafer and the PDMS side of the assembly was covered with Scotch™ removable tape.

c. Evaporation layer (EL) fabrication. The EL was fabricated out of NOA–81 thiolene (Norland Products) as described in previous work with several modifications.[53–55] Thiolene allows for replication of sub-micron features, as well as features with large aspect ratios due to its higher elastic modulus compared to PDMS. Thiolene is optically translucent enabling imaging *via* optical microscopy.[55] Fig. 2c provides an overview of the fabrication steps employed to create the EL. Positive photoresist (SPR 220-7, Rohm and Haas Electronic Materials) was patterned on a 4″ silicon wafer. Microchannels, 50 or 100 μm tall, were etched in the wafer by deep reactive ion etching (DRIE, PlasmaTherm ICP-DRIE etching system) for 30 min or 1 h. Next, the photoresist was washed away with acetone and the residual impurities on the wafer were removed by oxygen plasma (RIE, March Jupiter III). The etch depth was confirmed by profilometry (KLA Alphastep IQ). The etched wafer was coated with a monolayer of silane. Then a PDMS replica was prepared by pouring 5 : 1 A/B PDMS onto the etched silicon wafer and cured by heating in a convection oven (Thermo Scientific) at 65 °C for 1–2 h. The resulting PDMS mold was lifted off from the etched silicon wafer and a 3″ × 2″ PDMS window frame (10 : 1 A/B PDMS), ~2 mm in height, was reversibly sealed on the side of the PDMS mold with embossed features. The resulting structure will allow for replication of the embossed features in thiolene. The inner dimensions of the PDMS frame will define the outer dimensions (overall size) of the thiolene replica. Liquid thiolene was pipetted into the PDMS mold while avoiding the formation of bubbles, until it was completely filled to the edge of the frame. A microscope slide was placed on top of the PDMS mold to remove any excess thiolene and to provide rigidity. The liquid thiolene was then cured by UV exposure (OAI flood exposure system; intensity 10.8 mW cm^{-2}) for 6–10 min on one side, and then flipped and exposed again for another 6–10 min.[56] The glass slide bonds to thiolene upon curing and ensures that the formed, patterned thiolene layer remains flat and rigid. The thiolene layer, still bonded to the glass slide, was then removed from the PDMS mold.

d. Alignment and final assembly of all layers to obtain the complete chip. First, the IL was placed on the EL so the location of through-holes needed to connect the evaporation chambers in the TLA and the corresponding evaporation channels in EL could be marked. Then, after removing the EL, holes were drilled in the marked locations of the IL (Dremel 300 series, 100 μm McMaster-Carr drill bit). Next, the IL is manually aligned and reversibly sealed with the EL. Finally, the TLA is manually aligned and reversible sealed with the IL-EL assembly such that the holes in the evaporation chambers in the FL were aligned with the corresponding evaporation channels. These alignment steps are performed under an optical microscope (Leica MZ6) for accuracy. These alignment steps complete the fabrication and assembly of the complete chip for salt screening *via* evaporative crystallization. Fig. S1, ESI† shows detailed views of the assembly of different layers of the chip for evaporation driven crystallization experiment.

Preparation of parent compound (PC) and salt former (SF) solutions

All PCs and SFs were obtained from Sigma-Aldrich and used as received. The methanol solution of ephedrine (1 M) was prepared by dissolving 165 milligrams of ephedrine in 1 mL of methanol in a glass vial by vortexing (Maxi Mix II, Barnstead/Thermolyne). Six acids (hydrochloric, methane sulfonic, ethane sulfonic, sulfuric, nitric and phosphoric acids) were dissolved in methanol at a concentration of 2.4 M, such that SF and ephedrine are mixed on-chip with a molar ratio of 1.2 : 1.

Tamoxifen solutions were prepared following the same procedure. Tamoxifen was dissolved in ethanol at a concentration of 120 mM, close to its solubility in ethanol. Aqueous solutions of five solid acids (citric, tartaric, benzene sulfonic, fumaric, and succinic acid) and one liquid acid (methane sulfonic acid) were prepared at molar concentration of ~0.29 M, such that SF and tamoxifen are mixed on-chip with a molar ratio of 1.2 : 1.

Filling and mixing of the solutions in the microfluidic chips

All solutions are introduced into the chambers within the chip following a similar procedure as described previously for a 48-well microfluidic platform for cocrystal screening of PCs.[52] Each inlet corresponding to a PC or SF solution is connected *via* tubing (30 AWG thin-walled PTFE, Cole Parmer) to a 0.65 mL micro-centrifuge vial (VWR International) filled with a PC or a SF solution. To avoid solvent evaporation from the centrifuge vials, the tubing is inserted through 1-mm holes drilled into the vial caps. The solutions are introduced to the chambers on-chip upon actuation of the appropriate set of valves (*vide infra*) while simultaneously applying gentle suction at corresponding fluidic outlets. Once filled, the PC and SF solutions are allowed to mix for about an hour. After the solutions were fully mixed, peripheral connections such as tubing for filling were disconnected, the inlets and outlets of the chip were sealed, and all the fluidic inlets and outlets were covered with Crystal Clear Tape (Hampton HR4-511) to inhibit solvent loss. Finally, the valves that allow for evaporation were

actuated to allow solvent to escape through the evaporation channels and thereby initiate the evaporation driven crystallization experiments.

Visualization of the crystallization experiments

Throughout the mixing period (about an hour) and the subsequent evaporation period (up to 50 h), the wells were periodically monitored for appearance and growth of solids using an automated imaging system comprised of an optical microscope (Leica Z16 APO) equipped with an auto-zoom lens (Leica 10447176), a digital camera (Leica DFC280), and a motorized X–Y stage (Semprex KL66) controlled by Image Pro Plus 7.1 software (Media Cybernetics). Images of each well were acquired every 10 min by moving the automated motorized stage in a sequential manner from well to well. At the end of each experiment, after removing the highly birefringent EL, dark field images of each well were acquired using crossed polarizers to confirm the crystalline nature of the resulting solid forms.

Estimation of solvent evaporation rates

The moving solvent interface in each microfluidic well was recorded at designated time points using the images captured *via* time-lapse optical microscopy and analyzed (''freehand selection'' tool in ImageJ 1.46). The area and hence the volume (as the height of each well remains constant) occupied by the solution in each well was determined as a function of time. The rates of solvent evaporation were represented by the change in the volume fraction of the residual solution in each well.

Crystallization off-chip

Salt formation of ephedrine and tamoxifen was executed in glass vials to obtain reference solids for comparison with on-chip crystallization results. The off-chip experiments were conducted in 1-mL glass vials (Kimble/Chase). First solutions of ephedrine in methanol and tamoxifen in ethanol were prepared. Subsequently, the SF solutions were prepared in either methanol (for ephedrine) or water (for tamoxifen) at a molar concentration that ensured 1 : 1.2 molar ratio of PC : SF on mixing of 400 μL of PC solution with 200 μL of SF solution. 400 μL of PC solution was mixed with 200 μL of SF solution to maintain the 2 : 1 volumetric ratio of the PC and SF chambers on-chip. The solutions prepared in the vials were mixed *via* vortex followed by sonication for 5 min (Branson 2510). Each vial was then covered with parafilm (PARAFILM® M) having a hole through which solvents can evaporate slowly (in the range of 6–24 μL h^{-1}). The vials were then monitored for solid form formation and solvent evaporation over a period of 12–72 h. After complete evaporation of the solvent from the glass vials, the solid form crystallized in each vial was analyzed using optical microscopy (bright field as well as dark field) and Raman spectroscopy.

Solid form analysis

The glass vials (off-chip) were examined under a microscope to determine the crystalline nature of the solids collected in the experiments. To analyze the solids formed on-chip, the thiolene layer was peeled off the TLA–IL assembly after the completion of on-chip crystallization experiments (after 8 to 50 h). The crystalline nature of the solids in the TLA-IL assembly was verified using a stereomicroscope (Leica MZ12.5) equipped with a digital camera (Leica DFC295) under bright field as well as dark field using crossed polarizers (birefringence analysis).

The identity of each of the crystalline solid forms of ephedrine and tamoxifen was verified by a Raman spectrometer equipped with a 785 nm excitation source (Renishaw NIR 100 mW diode laser) and connected to an upright microscope (Leica DM2500M). The microfluidic chip was placed in the sample holder and individual wells were centered in the bright field mode using 5× magnification (Leica 506302 objective, 5×/0.12 NA), followed by use of higher magnifications such as 20× (Leica 566066 objective, 20×/0.4 NA) and/or 50× (Leica 566027 objective, 50×/0.75 NA). The laser was then switched on and set at 10% laser power and the Raman spectra of individual crystals were collected in the range of 600–1800 cm^{-1} for tamoxifen and 400–1700 cm^{-1} for ephedrine by focusing the laser beam to a spot size of ~5 μm at 50× magnification with a long working distance objective (Leica 566036 objective, 50×/0.5 NA) in the dark field mode.

The crystalline solids obtained off-chip were transferred onto a gold-coated glass slide for Raman analysis. Raman spectra of the solids were collected at 20× magnification and compared with those reported.[27,57] Gold coated glass slides were prepared by coating pre-cleaned microscope slides (Fischer Scientific 12–550-A3) with a 20-nm layer of chromium for adhesion, followed by deposition of a 200-nm layer of gold using an E-beam evaporation system (Temescal six pocket E-Beam Evaporation System). Data collection was carried out at a spectral resolution of ~0.5 cm^{-1} at 1800 gratings/mm, with the exposure time set to 40 s, and each spectrum was averaged over two accumulations.

Results and discussion

Chip design

The microfluidic chip reported here improves on the capability of the microfluidic chip we have reported previously for the mixing of small volumes of PC and SF solutions on-chip *via* FID in a combinatorial fashion.[27,52] The microfluidic platform reported here has 24 wells, each comprising of a PC chamber, a SF chamber, and an evaporation chamber (Fig. 1). Each well is isolated from the rest of the wells using a series of normally closed valves.[28] This platform can be used for combinatorial salt screening of a PC at 24 unique conditions: 1 PC solution × 6 salt former (SF) solutions at 4 different evaporation rates.

The volume of the PC chamber of each well is ~ 200 nL. When using PC solutions at a concentration of 50 mg mL^{-1}, only ~10 μg of PC is consumed for each crystallization condition investigated on-chip, which is two to three orders of magnitude less compared to the quantity of PC consumed per condition for a traditional off-chip screening approach (~ 600 μL solution per condition). Alcohols, especially methanol and ethanol, are most commonly used to dissolve the PC because

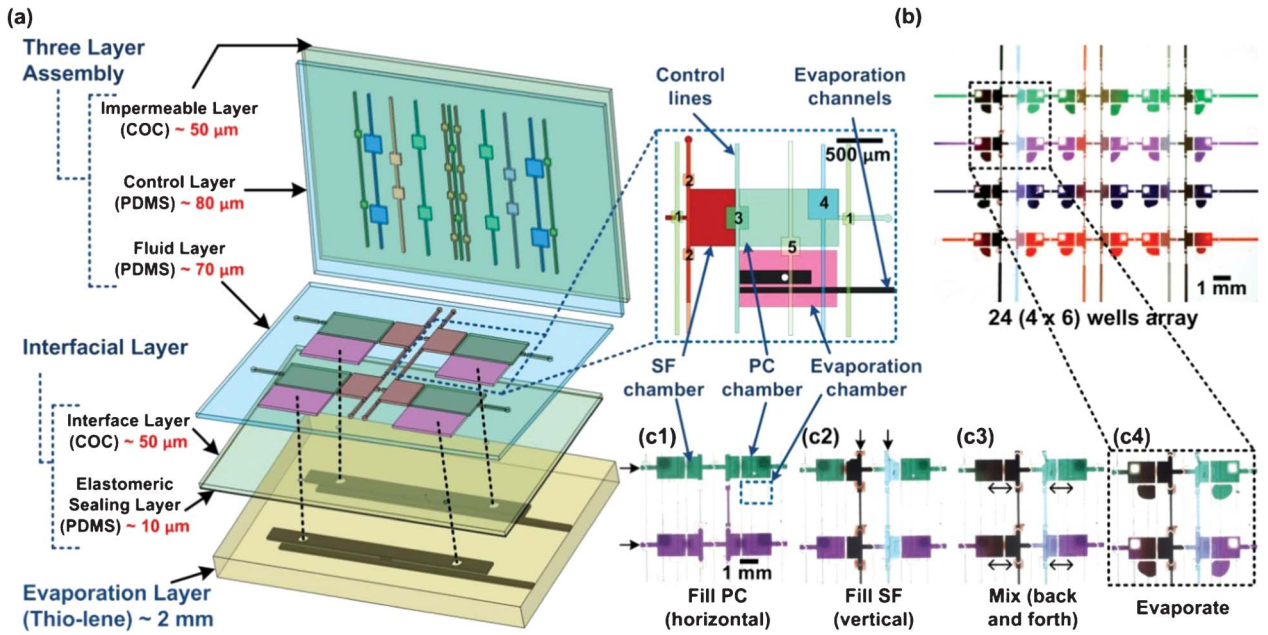

Fig. 1 (a) Schematics of the layered design of a 2 × 2 array of wells in a microfluidic crystallization chip. The top section, referred to as the *Three Layer Assembly* comprised of an *Impermeable Layer* that minimizes solvent loss and provides rigidity, a *Control Layer* with pneumatic control lines and valves to enable fluidic routing and mixing, and a *Fluid Layer* with three chambers per well: two for PC and SF solutions and one that allows for solvent evaporation after mixing. An *Interfacial Layer* which ensures reversible sealing and allows for compatibility with Raman spectroscopy, connects the *Three Layer Assembly* with the bottom section, the *Evaporation Layer*, which contains the channels that allow solvent to evaporate at a certain rate. (b) Optical micrograph of the evaporation based microfluidic crystallization screening chip comprised of a 4 × 6 well array, filled with dyed solutions to highlight the chip's combinatorial mixing capabilities. (c1–4) Enlarged views of a 2 × 2 array of wells to visualize chip operation: PC solutions are introduced horizontally (valves 1 and 3 actuated) and locked up in the PC and SF chambers (c1). SF solutions are introduced vertically (valves 2 actuated) and locked up in their respective chambers after the PC solutions are purged from these SF chambers by applying vacuum at the outlets (c2). Adjacent PC and SF solutions are mixing (valves 3 actuated) (c3). Back-and-forth movement of solutions (repeated actuation of valves 4) can be used to speed up the mixing process. The mixed solutions are then allowed to concentrate *via* solvent evaporation through the microchannels in the Evaporation Layer (valves 5 actuated) (c4).

PCs generally dissolve well in these solvents. However, when PCs are poorly soluble in alcohols, the success of the experiment may be jeopardized due to insufficient availability of PC in each PC chamber. This potential limitation was partially overcome in the platforms reported here by increasing the well volume of the PC chamber by a factor of 2.25 compared to well volume in the FID-based microfluidic chips reported earlier.[27,52]

Most of the pharmaceutically acceptable SFs that are most commonly used in early stage solid form screening, are small molecules and have high solubility in alcohol and water. Hence, high concentrations of the SF solutions can be introduced in the SF chambers on-chip. Therefore, the size of the SF chamber is designed to be half the size of the PC chamber, which allows the SF and PC to be mixed at equimolar ratio. In practice, PC and SF solutions are frequently prepared in organic solvents and water, respectively. The smaller size of the SF chamber compared to the PC chamber reduces the chance of precipitation of PC upon mixing with aqueous solutions of SF due to antisolvent effects.

The solutions of PC and SF are mixed on-chip by diffusion. The time required to achieve complete mixing depends on the diffusivity of each component as well as the dimension of the chambers. The distance that a component travels by diffusion within a time t can be estimated using Fick's law, $l = 2(Dt)^{1/2}$. The combined length of the SF and the PC chambers was approximately 2.7 mm. The diffusivity D of the molecules used here is on the order of 10^{-9} m^2 s^{-1}. Therefore, the solutions of PC and SF will be completely mixed by diffusion in approximately one hour after the onset of mixing.

A third chamber, an evaporation chamber, was added to the fluid layer adjacent to each PC chamber. The evaporation chamber was connected to the PC chamber (containing the mixed PC/SF solutions) through a control valve. The evaporation chamber was further connected to the atmosphere *via* evaporation channels in the EL, through which the solvent vapor can diffuse to the outside environment. The rate of solvent evaporation is determined by the dimensions of the evaporation channels. The rate of solvent evaporation can be expressed by the following equation:[16,20,58]

$$J = \frac{DM}{RT}\Delta P\frac{A_C}{L} \quad (1)$$

where

J is the volumetric flow rate of solvent evaporating out of the chamber

ΔP is the difference between the partial pressure of the solvent mixture in the evaporation chamber and that of the ambient, the atmosphere outside the chip

D is the diffusivity of solvent vapor in air

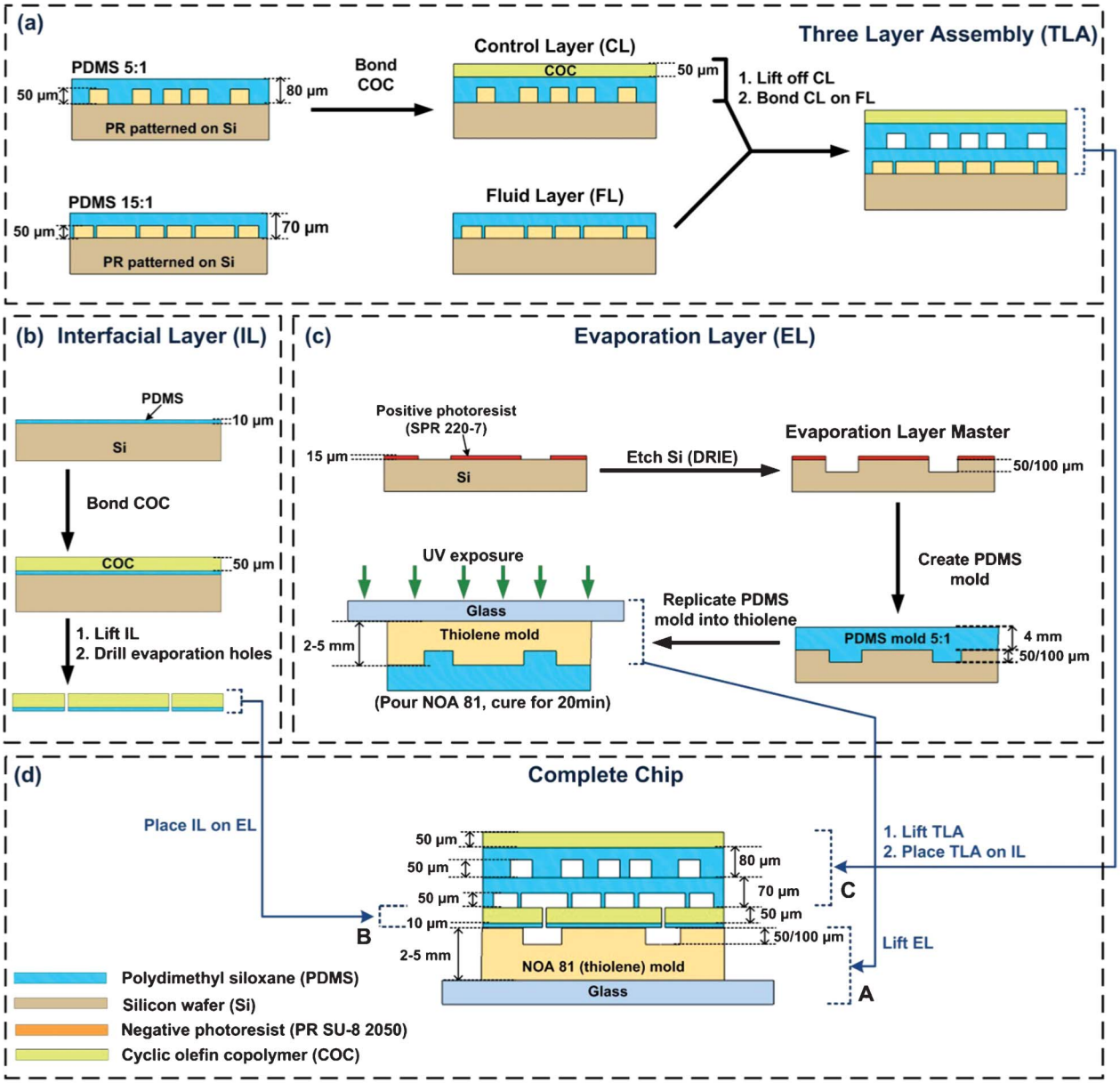

Fig. 2 Fabrication steps for the evaporative crystallization chip. (a) Negative patterns for the control layer (CL) and the fluid layer (FL) are patterned on Si-wafers, which are replicated in PDMS to obtain the FL and CL, and a cyclic olefin copolymer (COC) sheet is irreversibly bonded (plasma) to the CL. Then the COC-CL assembly is lifted off the master and sealed with the FL *via* thermal curing to yield the TLA. (b) The IL is obtained by spin coating and curing a thin layer of PDMS on a silanized Si-wafer, plasma bonding of a COC sheet, and lift off from the Si substrate. (c) The EL is created by first creating an appropriate master *via* photolithography and DRIE, followed by replication to obtain a PDMS mold, which in turn is replicated in thiolene by applying the liquid pre-polymer and subsequent UV curing. (d) Chip assembly is completed by placing the IL on the EL, and then placing the TLA on the IL-EL assembly.

M is the molecular weight of the solvent mixture
R is the gas constant
T is the absolute temperature
A_c is the cross-sectional area of the evaporation channel
L is the length of the evaporation channel.

The evaporation rate of the solvent selected in the experiment is proportional to the difference in partial pressure, diffusivity of the solvent, and molecular weight of the solvent. The difference between the partial pressure of the solvent in the evaporation chamber and that of the ambient serves as the driving force for the evaporation of the solvent. The partial pressure of the solvent of the ambient remains constant, *i.e.* zero for the organic solvent, and equal to the relative humidity for water (assuming it does not change during the experiment). The concentration of the solute increases as the solvent is removed *via* evaporation. Thus, the partial pressure of the solvent in the evaporation chamber decreases with time. However, the change in the partial pressure of the solvent in the chamber can be ignored in cases where precipitation occurs before the solution becomes too

concentrated. Therefore, we can consider that the driving force for solvent evaporation remains constant during the experiment.[17]

When a particular solvent is selected for the experiment, the evaporation rate can be controlled by the dimension of the micro-channels, as previously reported for PDMS and polypropylene platforms for droplet based crystallization.[16] Eqn (1) suggests that the evaporation rate increases if the evaporation chamber is connected to a shorter evaporation channel having a large cross-sectional area. The evaporation channels in the EL were designed such that the solvent in the 6 wells in the same row in a 4 × 6 microfluidic array chip evaporated at the same rate, while each row results in solvent evaporation at a unique rate. In addition to solvent evaporation through the evaporation channels, solvent loss can also occur due to solvent absorption by the chip materials, followed by evaporation of solvent to the outside of the chip. As a control experiment, we always filled six wells in one of the four rows in the microfluidic chip without connecting them to an evaporation channel. This allowed us to determine the rate of solvent loss due to absorption. An optical micrograph of the complete assembly of the microfluidic chip highlighting the evaporation channels is provided in the Supplementary Information (Fig. S2, ESI†).

The rate of solvent loss in the microfluidic chips can be represented by the volume fraction of residual solvents in the chambers as a function time (see Fig. S3, ESI†). Pure methanol escaped from the control wells at a rate of 4 nL h^{-1} and from the wells in the other three rows at a rate of 16, 10, and 7 nL h^{-1}, respectively. Thus, the rates of evaporation of methanol from the wells in the three rows connected to evaporation channels, adjusted for the control, are 12, 6, and 3 nL h^{-1}. These experimentally determined rates are slightly smaller than the expected rates, calculated using eqn (1), *i.e.*, 15, 7.5, and 3.75 nL h^{-1}, respectively.

The rate of evaporation of water from the control wells (closed, no evaporation channels) was determined to be 1.2 nL h^{-1}. The observed rates of evaporation of water from the wells in the three rows connected to evaporation channels, adjusted for the control, are 2.4, 1.2, and 0.6 nL h^{-1}, which are close to the expected rates of 2.5, 1.5, and 0.625 nL h^{-1}, respectively. Water is a less volatile solvent and thus the loss of water through the chip material was minimal compared to the loss of methanol. The measured solvent evaporation rates were higher than the expected values. However, after adjustment for the solvent loss into or through the chip material, the solvent evaporation rates were in close agreement with the rates calculated using eqn (1).

Many other parameters, such as the location of the through holes in the evaporation chamber, the size of the hole, and the presence of a bubble trapped in the well, may affect the rate of solvent evaporation during the experiment. Nevertheless, the microfluidic chips provide good control over the evaporation rate of water with little well to well variation (less than 10%) in the same row of the chip. In contrast, well-to-well variation on the order of 20–40% was observed when using methanol as the solvent. This inconsistency is probably due to the higher volatility of methanol in combination with the chip material (PDMS) absorbing methanol to a higher extent than water.[51]

Solvent compatibility of chip

Based on prior work regarding the solubility of solvents in PDMS and the degree to which the solvent may swell PDMS,[51] we expect that the previously reported PDMS-based droplet evaporation platforms[15] and the standard multilayer PDMS platforms[22] are compatible with use of solvents such as water and various alcohols for crystallization screening experiments. However, as mentioned above PDMS does absorb these solvents to a certain extent, may swell by up to 9% in volume, and solvents may evaporate from the surface of PDMS.[51] These solvent loss mechanisms limit the time for crystallization experiments to less than 2 h (based on 200 nL droplets), thus hampering the use of all-PDMS chips for on-chip evaporative crystallization.

As in our prior work,[52] we minimize solvent absorption by the chip, by reducing the total thickness of the PDMS fluid and control layer to ~160 μm, and sandwiched the PDMS layers between two 50-μm COC layers, which are much less permeable (compared to PDMS layers) to the solvents of interests and swells less when in contact with these solvents.[59] These improvements significantly minimized solvent loss resulting from materials comprising the TLA-IL assembly while using organic solvents, including volatile alcohols such as methanol, ethanol, isopropanol, trifluoroethanol, and acetonitrile. The solutions were retained in the chambers on-chip for more than 12 h when the wells were isolated from the ambient. Beyond our prior work, an evaporation layer (EL, Fig. 1) is applied to the chip enabling evaporative crystallization at designed solvent evaporation rates. This layer is made out of thiolene, a material that is impermeable to air and solvent-vapor, and has superior resistance to a wide range of solvents (*e.g.*, toluene, benzene).[60]

Raman compatibility of chip

Various analytical techniques such as X-ray diffraction (powder and single crystal X-ray), solid state NMR, IR (including near IR and Fourier transform IR) spectroscopy, and Raman spectroscopy are typically used to identify the crystal forms of organic molecules.[57,61–63] Here, we used Raman spectroscopy for on-chip as well as off-chip solid form identification due to its chemical specificity, high throughput, amenability to automation, and high spatial resolution thus reducing sample needs.[57] As for our previously reported FID-based microfluidic platforms,[52] the layered assembly of this PDMS fluid and control layers, sandwiched by thin COC layers used here (the TLA-IL assembly), ensured sufficient transparency and signal to noise ratios to permit analysis of solid forms using Raman spectroscopy. Only the non-Raman-transparent EL needs to be removed at the end of the evaporation experiment (See Fig. S1, ESI†). The ESI file provides Raman spectra of COC, PDMS, and an assembled TLA-IL assembly (Fig. S4, ESI†), as well as the process of background correction of on-chip Raman spectra (Fig. S5, ESI†).

Chip operation

Fluidic routing and mixing on-chip is controlled using an array of normally closed valves (five sets) incorporated in the control layer (Fig. 1).[28,52] The PC solutions are introduced along the

rows into the PC and SF chambers upon actuation of the valve sets labeled "1" and "3" *via* application of vacuum at the control line inlets and application of vacuum at the outlets (Fig. 1c1). Next, valve sets 1 and 3 are closed to isolate PC solution in the PC and SF chambers, and the SF chambers are emptied by actuating valve set 2 and applying vacuum at the corresponding outlets. Then, the SF chambers are purged with the solvent employed for the PC solutions, and SF solutions are introduced into the SF chambers by gentle vacuum suction at the outlets (Fig. 1c2). Valve set 2 is then closed to isolate the PC and SF solutions in adjacent chambers. The solutions are mixed by natural diffusion for approximately an hour by continuous actuation of valve set 3. Valve set 4 is actuated occasionally to push the solutions back and forth between the chambers for a better mixing (Fig. 1c3). After the solutions are fully mixed, all peripheral connections except the pneumatic tubing to actuate valve set 5 is removed, and the chip is sealed with Crystal Clear Tape to prevent solvent evaporation through the inlets and outlets. Upon actuation of valve set 5 (Fig. 1c4), the mixed solutions in the PC chamber are then exposed to the ambient through the evaporation channels in the EL to allow for solvent evaporation at the designed rates. After completion of the experiment, valve set 5 is closed by releasing the vacuum, thereby isolating the PC chambers, SF chambers, evaporation chambers, and the feed lines. The chip can be disconnected from the only remaining tubing, enabling easy handling and transport to solid form analysis stations (*i.e.*, optical microscope and Raman microscope).[27]

Salt screening experiments

Ephedrine and tamoxifen (both bases), two commercially available drugs, were used for validation of on-chip salt screening. Each of these two PCs was mixed combinatorially with several SFs in 24-well chips to screen for crystalline salts. During crystallization screening, the wells were monitored for crystal formation using a bright field microscope.

Ephedrine salt screening

We conducted salt screening of ephedrine with various acids using the developed microfluidic chip. Methanol solution of ephedrine (1 M) was introduced along the four rows of the chip (each row corresponding to a different evaporation rate of solvent). Methanol solutions of six acids, *i.e.*, ethane sulfonic, hydrochloric, methane sulfonic, nitric, phosphoric, and sulfuric acids (2.4 M) were introduced along the six columns. Ephedrine is known to form salts with these acids.[64,65] Solutions of ephedrine were mixed with the acid solutions on-chip in a combinatorial fashion. The molar ratio of ephedrine and acid in each mixture was 1 : 1.2. No solid formation was observed during the mixing of the ephedrine and SF solutions on-chip (~one hour). The same solution mixtures prepared in 1 mL glass vials (off-chip) and left for 24 h did not exhibit solid forms. These observations suggest that the solution mixture was under-saturated with respect to each component forming the salt and the intended salt. After complete mixing of the solutions on-chip, they were then concentrated with respect to all the components (PC, SF, and the intended salt) as the solvent was removed through the microchannels in the EL at the rate of 16.6 $\pm$ 2, 11 $\pm$ 1.5, and 8.3 $\pm$ 1.2 nL h^{-1}. A row of wells without an evaporation channel, for which the rate of solvent loss through the chip material was about 5.8 nL h^{-1}, was used as a control experiment.

As the solvent evaporation progressed, on-chip salt screening resulted in crystalline solids in all conditions as shown in Fig. 3 and Table 1. Fig. 3 shows an optical micrograph of a whole 24-well chip during ephedrine salt screening, after the EL had been removed. Fig. S2, ESI† shows the complete 24-well chip during ephedrine salt screening with the evaporation channels highlighted. Raman spectroscopy confirmed that the intended salts were obtained in the presence of all six acids. The onset of crystallization was found to depend on the SF used in the on-chip experiment: 1.5–4 h with phosphoric acid and sulphuric acid (with different evaporation rates), 8–13 h with methane sulfonic acid, hydrochloric acid, and ethane sulfonic acid, and 18–24 h with nitric acid. We computed the final concentration of each salt in solution at the onset of crystallization and observed that different salts started to crystallize at different concentrations, which is probably due to difference in the solubility of the salts. As expected, the crystallization of each salt of ephedrine occurred at an earlier time point in the chambers in which solvent was evaporated at higher evaporation rates. Crystallization was always encountered at a later time in the control experiments where supersaturation was induced only *via* solvent absorption into chip materials. The observed trends in on-chip crystallization onsets confirm the ability of the chip to expose different wells to different, predetermined rates of evaporation.

The 100% success rate achieved in this study (every condition yielded a crystalline form, see Fig. 3 and Table 1) presents an advantage of on-chip evaporative crystallization over reactive crystallization off-chip after instantaneous mixing as well as on-chip crystallization *via* free interface diffusion (FID) which we reported previously.[27] In our prior work, concentrated solutions of ephedrine and SFs (five times more concentrated than the concentrations used in this study) were mixed on-chip to achieve high levels of supersaturation in the resulting solution. The on-chip experiments using the reactive crystallization mode resulted in the crystallization of five salt forms, with no solid formation observed in the presence of nitric acid. The high degree of supersaturation achieved in the previous study achieved *via* mixing of concentrated solutions of ephedrine and nitric acid might have resulted in the precipitation of non-crystalline solid or the formation of a gel over a period of time, even though the increase in the supersaturation level resulting from solvent loss through the chip material in the previous study was gradual and similar to the rate of solvent loss through the chip material in the evaporative crystallization chips used here.

The evaporation-based microfluidic chips allow each component of a salt to mix through diffusion followed by the evaporation of solvent. Various supersaturation levels are traversed at different rates over a 12 to 48 h timespan, which, compared to non-evaporative on-chip and off-chip crystallization screening methods, significantly improves the success

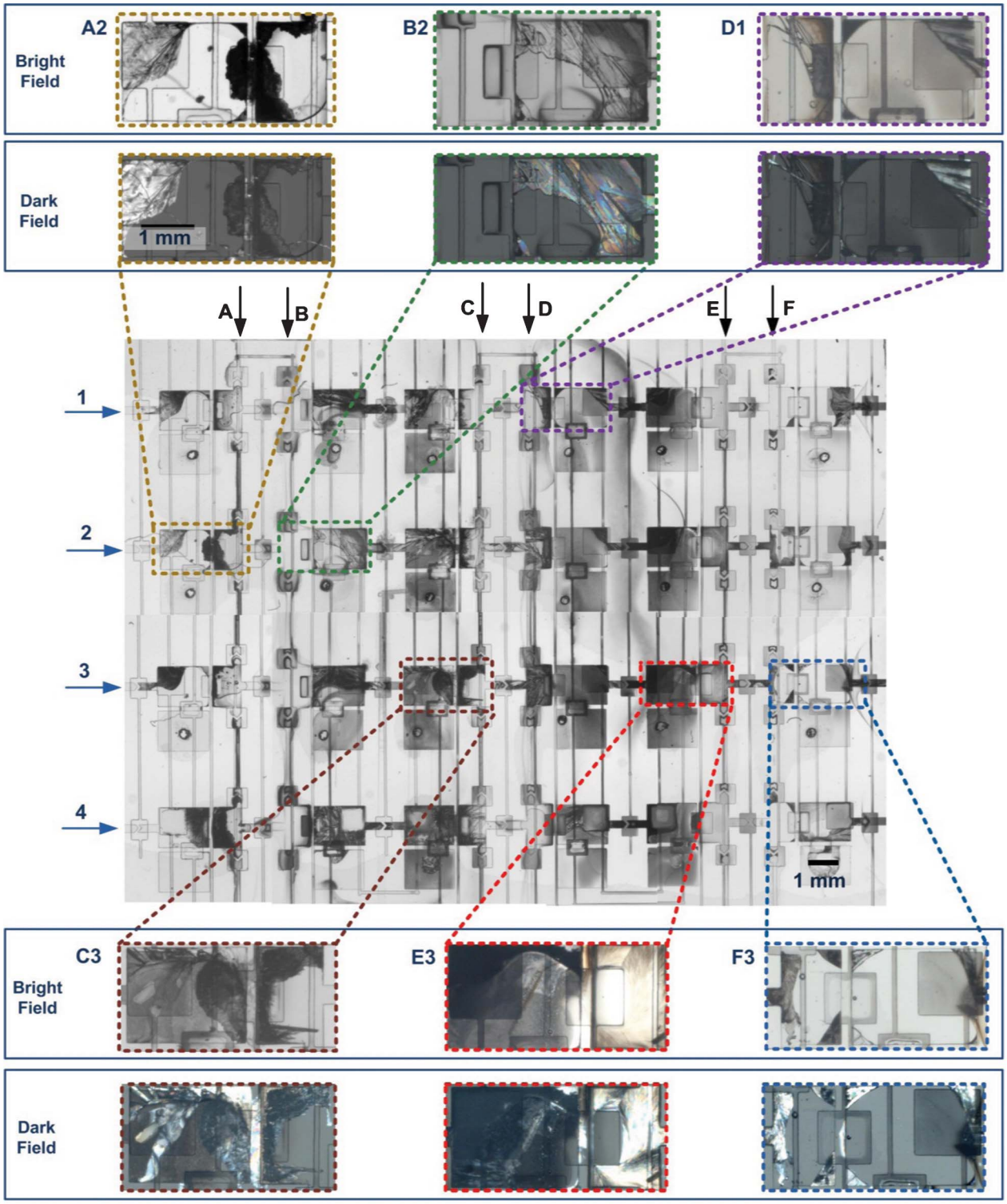

Fig. 3 Tiled optical micrograph of the chip (after removal of the EL) for an on-chip screen of salt solid forms of ephedrine. Rows 1, 2, 3, and 4 are filled with 1 M ephedrine dissolved in methanol. The columns are filled with 2.5 M solutions of the following SFs prepared in methanol: phosphoric acid (A); methane sulfonic acid (B); sulfuric acid (C); ethane sulfonic acid (D); hydrochloric acid (E); and nitric acid (F). *Enlarged views at the top and bottom*: Bright field and dark field (crossed-polarizers) images of the dihydrogen phosphate (A2), mesylate (B2), bisulfate (C3), esylate (D1), hydrochloride (E3), and nitrate (F3) salts of ephedrine.

rate of salt screening as evident from Table 1. In the FID-based reactive crystallization chips, when the concentrated solutions are mixed upon opening the valves between the PC and SF chambers crystallization often occurs at the location of the valve due to the occurrence of instantaneous, extremely high levels of supersaturation, disrupting the designed experiment

Table 1 Distribution of the various solid forms of ephedrine identified on-chip

		Crystal forms of ephedrine					
Crystallization data from Fig. 3		Dihydrogen Phosphate	Mesylate	Sulfate	Esylate	Hydrochloride	Nitrate
Rate of solvent evaporation (nL h^{-1})	16.6 ± 2	E-DP[a]	E-M	E-BS	E-E	E-H	E-N
	11 ± 1.5	E-DP	E-M	E-BS	E-E	E-H	E-N
	8.3 ± 1.2	E-DP	E-M	E-BS	E-E	E-H	E-N
	5.8 ± 0.8	E-DP	E-M	E-BS	E-E	E-H	E-N
		Crystal forms of tamoxifen					
Crystallization data from Fig. 5		Benzene sulfonate	Succinate	Fumarate	Citrate	Tartrate	Mesylate
Rate of solvent evaporation (nL h^{-1})	14.8 ± 2.6	T-BS	×[b]	T-F	T-C	T-T	T-M
	9.5 ± 1.2	T-BS	×	T-F	T-C	T-T	T-M
	7.4 ± 1.2	T-BS	T-S	T-F	T-C	T-T	T-M
	5.2 ± 0.8	T-BS	T-S	T-F	T-C	T-T	T-M

[a] Salt forms: Ephdrine dihydrogen phosphate (E-DP), mesylate (E-M), bisulfate (E-BS), esylate (E-E), hydrochloride (E-H), and nitrate (E-N); Tamoxifen benzene sulfonate (T-BS), succinate (T-S), fumarate (T-F), citrate (T-C), tartrate (T-T), and mesylate (T-M). [b] × indicates no crystalline solid formation.

with respect to diffusional mixing profiles and final concentrations. Furthermore, crystallization of the PC or the SF may often take place due to a change in solubility at the interface of the two solutions. In the evaporation-based chips, crystallization does not occur upon onset of mixing when opening the valve between the PC and SF chambers because usually more dilute solutions of PC and SF are used. Crystallization can take place anywhere in the entire chamber. Indeed crystals typically formed along the corners and sidewalls of the microfluidic chambers. As the solvent evaporation progresses, the solvent interface retracts and the remaining solution gets more concentrated. Such concentration of the solution results in crystallization of the solid forms away from the point of contact of solutions and thereby avoids disruption of the crystallization experiment. Fig. 4 shows time-lapse optical micrographs of the evaporation of the solvent mixture and crystallization of solid form of ephedrine with phosphoric acid as the time progresses in the case when solvent evaporates at ~16.6 nL h^{-1}.

Crystallization using the evaporation-based microfluidic chips also demonstrated their advantage over the manual, conventional scale evaporation experiments. Initial off-chip crystallization only resulted in three salts when the solution mixtures (~600 μL) were allowed to evaporate from open vials. Covering the vials with parafilm with a pinhole (~5 mm diameter) significantly slowed down the evaporation, therefore, improved the success rate of the crystallization. At these conditions, five of six salts of ephedrine crystallized over a

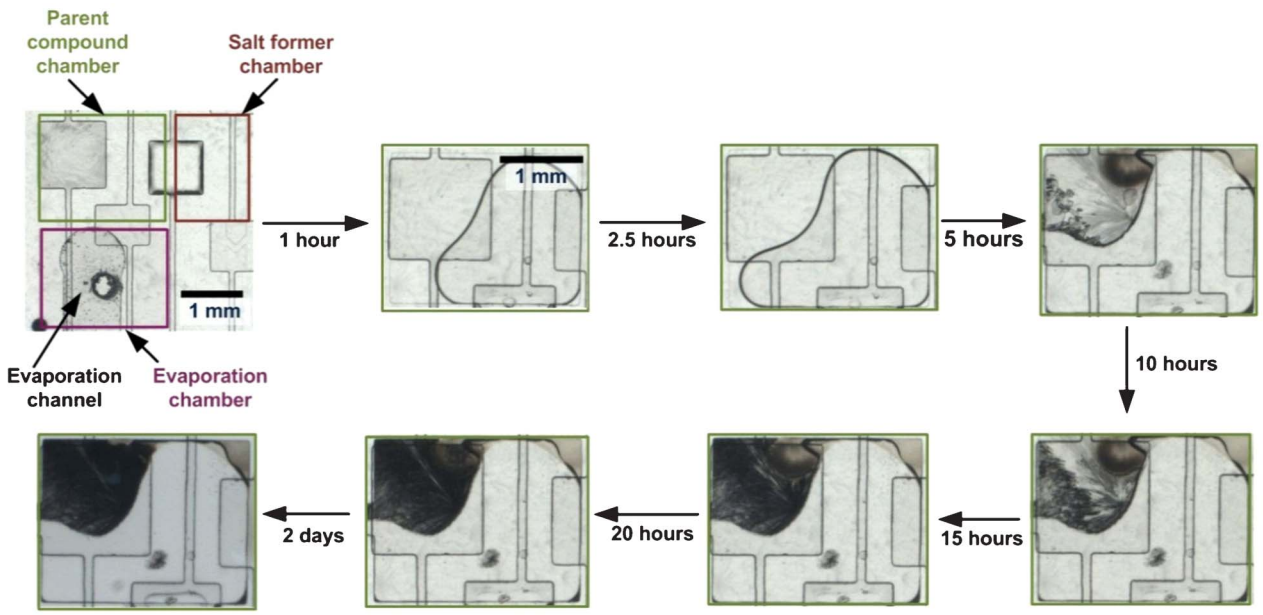

Fig. 4 Time lapse images of a single microfluidic crystallization chamber showing the gradual evaporation of the solvent from a mixture of ephedrine and phosphoric acid dissolved in methanol leading to crystallization of ephedrine dihydrogen phosphate salt crystals. The image represents an area of 1.9 by 1.5 mm^2.

period of 48 to 60 h. A gel still formed in the presence of nitric acid even when the glass vial was covered by a parafilm with a pinhole. The difficulty to crystallize ephedrine nitrate suggests that nucleation of this salt is slow and occurs only when the solution remains at certain supersaturation levels over a long period. We repeated the experiment several times by reducing the size of the pinhole on the covering parafilm. Crystallization only was observed when the diameter of pinhole was reduced to ~2 mm, at which condition the ~600 μL solution mixture evaporated in approximately 84 to 96 h. Evaporation-based microfluidic chips allow the solutions to traverse supersaturation levels at a controlled and low rate, which increases the chance of crystallization.

Fig. 3 shows representative examples of the crystals formed for each of these salts in the individual wells. Ephedrine crystallized as needles with ethane sulfonic acid, and as plates with methane sulfonic acid, sulfuric acid, nitric acid, and phosphoric acid. Both needles and plates were observed when ephedrine was crystallized with hydrochloric acid. These observations are in agreement with those reported in the literature.[65]

We observed that lower rates of solvent evaporation resulted in large (0.2–1 mm long) isolated crystals, whereas higher rates of evaporation led to accumulation of small crystals. These observations suggest that crystallization of these salts was nucleation controlled and the rates of crystal growth were higher than the rates of nucleation for each of the respective salts. On-chip crystallization experiments confirm that slow evaporation rates favor crystal growth and fast evaporation rates favor crystal nucleation, in accordance with predictions from crystal nucleation and growth theories.[66] As the solvent evaporation progressed, on-chip salt screening resulted in crystalline solids with all the SFs as shown in Fig. 5 and Table 1. Fig. 5 shows an optical micrograph of a whole 24-well chip during ephedrine salt screening, after the EL had been removed. As solvent evaporation progressed, tamoxifen crystallized with tartaric acid in 3–8 h (different solvent evaporation rates), with citric acid, fumaric acid, and methane sulfonic acid in 7–14 h, and with benzene sulfonic acid and succinic acid in 16–25 h. The difference in the crystallization onset was observed as a result of the difference in solubilities of the salts in the solutions. We also observed that the crystallization onset correlated well with that of the evaporation rate: crystallization occurred earlier for conditions where the evaporation rate was higher, and occurred at the latest time point in the case of the control experiment. This correlation suggests that all crystallization experiments were performed at well-controlled evaporation rates.

Tamoxifen salt screening

Salt formation of tamoxifen with six acids (benzene sulfonic acid, citric acid, fumaric acid, methane sulfonic acid, succinic acid, and tartaric acid) was also conducted using the evaporation-based microfluidic chip. Ethanol solutions of tamoxifen (120 mM) were mixed at room temperature with ~0.3 M aqueous solutions of each acid in combinatorial fashion in molar ratios of tamoxifen to acid of 1.2 : 1. Crystallization was induced by gradual evaporation of solvent through the microchannels in the EL at rates of 14.8 ± 2.6, 9.5 ± 1.2, or 7.4 ± 1.2 nL h^{-1}. Crystallization in the wells that were not connected to the evaporation channels was used as a control experiment. The rate of solvent loss in the closed control wells was about 5.2 nL h^{-1}. No crystallization was observed on-chip even one hour after to the onset of the mixing of the solutions. Similarly, the same solution mixture prepared in glass vials (off-chip) followed by 5-minutes sonication did not result in the formation of crystals within 24 h. These observations suggest that the intended salt as well as both components of the salt were under-saturated before the solutions were concentrated *via* solvent evaporation.

As solvent evaporation progressed, tamoxifen crystallized with tartaric acid in 3–8 h (different solvent evaporation rates), with citric acid, fumaric acid, and methane sulfonic acid in 7–14 h, and with benzene sulfonic acid and succinic acid in 16–25 h. The difference in the crystallization onset was observed as a result of the difference in solubilities of the salts in the solutions. We also observed that the crystallization onset correlated well with that of the evaporation rate: crystallization occurred earlier for conditions where the evaporation rate was higher, and occurred at the latest time point in the case of the control experiment. This correlation suggests that all crystallization experiments were performed at well-controlled evaporation rates.

Tamoxifen crystallized with all six different SFs used in this study. The succinate crystallized when the crystallization was conducted at two lowest evaporation rates, *i.e.*, 7.4 and 5.2 nL h^{-1}, but non-crystalline solids formed at two higher evaporation rates, *i.e.*, 14.8 and 9.5 nl h^{-1}. These observations suggest that the rate of nucleation of the succinate salt is very slow. When solvent was removed at higher rates, the solution became so concentrated that high viscosity prevented the crystallization of the salt before nucleation could take place.

Off-chip experiments in open glass vials, with ~600 μL volume per vial, only resulted in the crystallization of citrate, fumarate, and tartrate salts of tamoxifen. Slowing down the evaporation rates by covering the glass vials with a parafilm with a pinhole (~5–10 mm diameter) resulted in the crystallization of two more salts in about 48 h. Crystallization of the succinate was tried repeatedly off-chip, but only observed when the diameter of the pinhole in the parafilm was reduced to below 2 mm. In summary, the off-chip experiments yielded the same results as the on-chip experiments, but many more trials had to be performed (and thus much more sample has to be used) off chip in order to collect the same information.

Solid form analysis

Optical micrographs provide information about the size and morphology of any solid forms encountered in the microfluidic wells (See for example Fig. 6a), however, these images do not reveal the chemical identity of a crystal, which is important because crystals of the free PC and/or the free SF may form in addition to, or instead of, crystals of the desired salt. Fig. 6b and Fig. 7 show Raman data for the on-chip identification of the crystalline material formed in different wells. For reference, we recorded Raman spectra of all materials used in chip fabrication, as well as an empty TLA-IL assembly (Fig. S3, ESI†) and of all pure SFs as well as pure

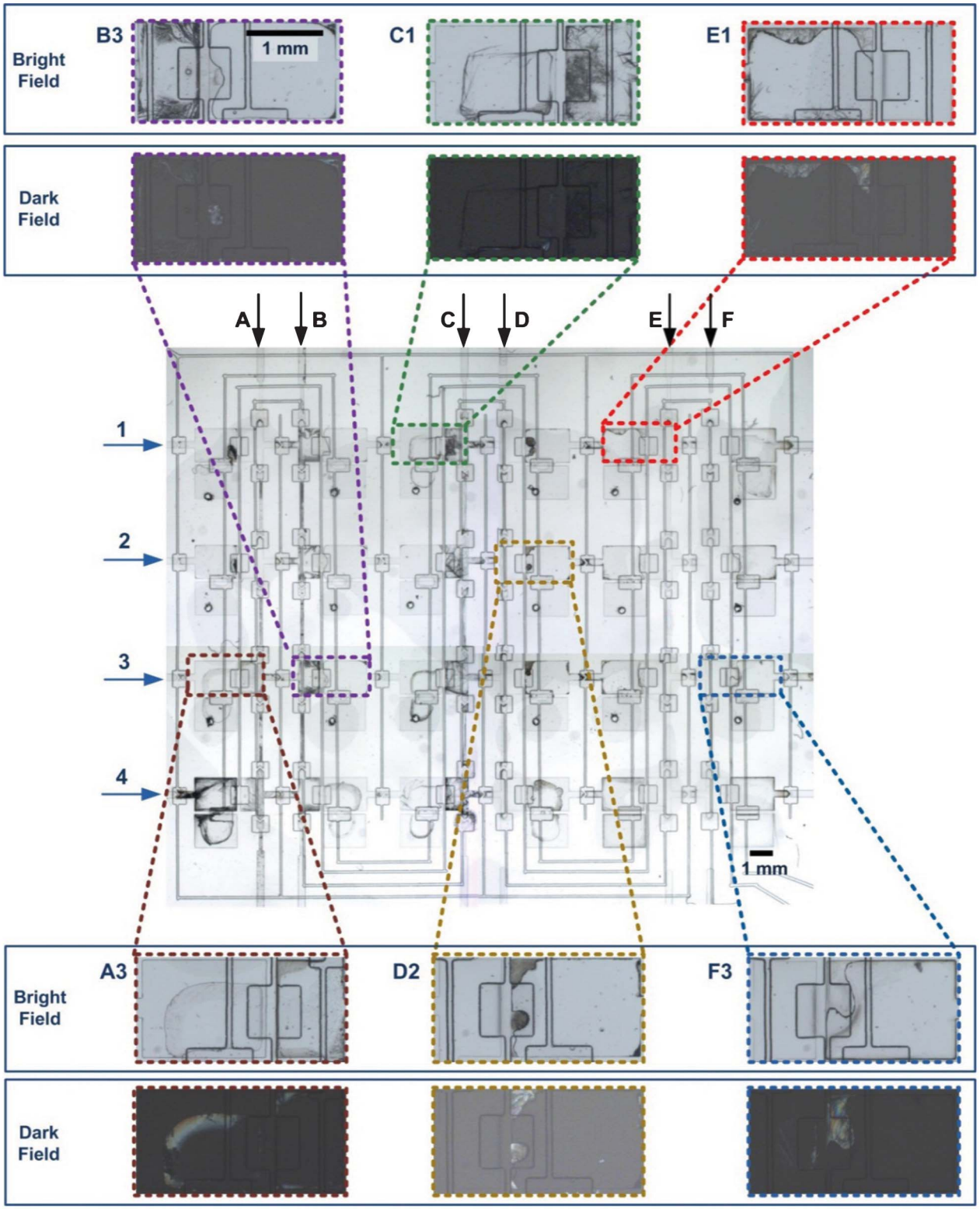

Fig. 5 Tiled optical micrograph of the chip (after removal of the EL) for an on-chip screen of salt solid forms of tamoxifen. Rows 1, 2, 3, and 4 are filled with 0.120 M tamoxifen dissolved in ethanol. The columns are filled with 0.25 M solutions of the following SFs prepared in water: benzene sulfonic acid (A); succinic acid (B); fumaric acid (C); citric acid (D); tartaric acid (E); and methane sulfonic acid (F). *Enlarged views at the top and bottom*: Bright field and dark field (crossed-polarizers) images of the benzene sulfonate (A3), succinate (B3), fumarate (C1), citrate (D2), tartrate (E1), and mesylate (F3) salts of tamoxifen.

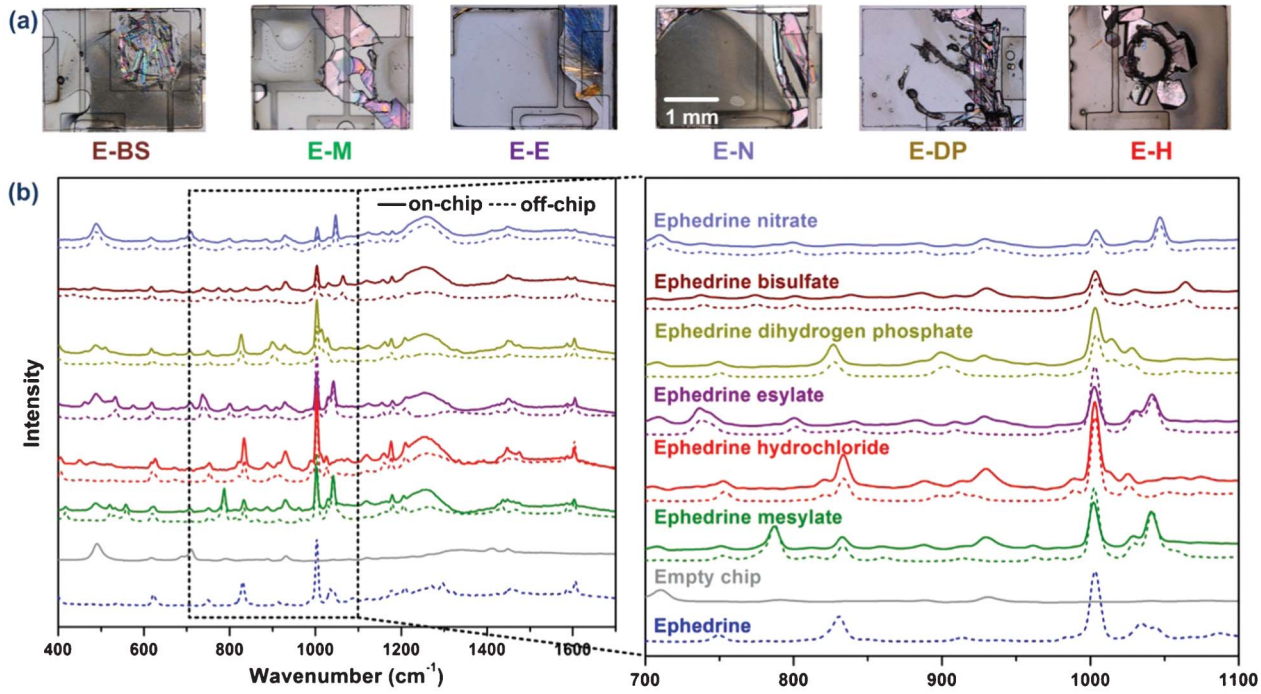

Fig. 6 (a) Magnified views of the some high quality crystals of different salt forms of ephedrine crystallized on-chip. Each image represents an area of 1.9 by 1.5 mm^2. (b) Raman spectra of ephedrine as well as different ephedrine salt crystals grown and analyzed on-chip (solid lines) and off-chip (dotted lines). The magnified views of the 700–1100 cm^{-1} range are provided to highlight the lack or presence of spectral differences between the different salts and/or samples grown on-chip and off-chip. ''Empty chip'' corresponds to the Raman spectrum of the TLA-IL assembly by itself.

PCs (Fig. S4, ESI†). Multiple individual crystals within each well were located and analysis on-chip.

The Raman spectra of the individual crystals were collected in the range of 400–1700 cm^{-1} and 600–1800 cm^{-1} for ephedrine (Fig. 6b) and tamoxifen (Fig. 7) solid form screening, respectively. The raw data was corrected for background from the chip (TLA-IL assembly). An example of the data correction process, one for solid form of ephedrine and the other for tamoxifen is provided in Fig. S4, ESI†. The Raman spectra of the crystalline solids formed in the on-chip experiments were in agreement with the reference Raman spectra from the salts obtained in off-chip experiments. The

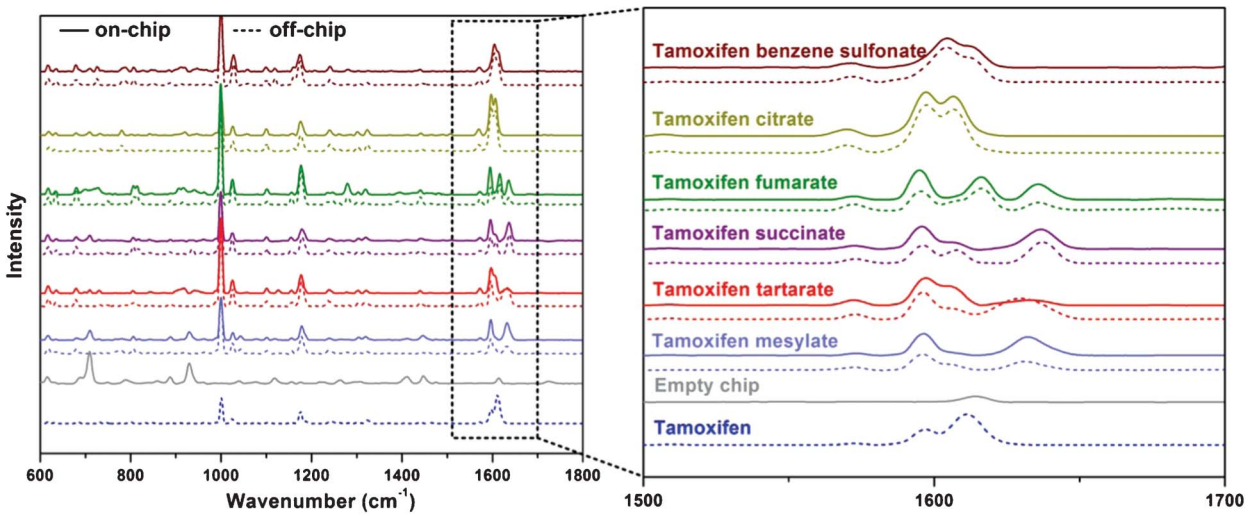

Fig. 7 Raman spectra of tamoxifen as well as different tamoxifen salt crystals grown and analyzed on chip (solid lines) and off chip (dotted lines). The magnified views of the 1500–1700 cm^{-1} range are provided to highlight the lack or presence of spectral differences between the different salts and/or samples grown on-chip and off-chip. ''Empty chip'' corresponds to the Raman spectrum of the TLA-IL assembly by itself.

unique peaks in the Raman spectra, seen in the magnified views of the 700–1100 cm^{-1} range for ephedrine (Fig. 6b) and the 1500–1700 cm^{-1} range for tamoxifen (Fig. 7), distinguished different solid forms from each other and from their respective PCs, and confirmed agreement between on-chip and off-chip data. The various identified crystalline salts of ephedrine and tamoxifen are summarized in Table 1. In addition, the Raman spectra for tartrate and citrate salts of tamoxifen obtained on-chip and off-chip were in good agreement with the Raman spectra for the same compounds reported elsewhere.[57] These results confirmed that the six salts of ephedrine and tamoxifen were successfully prepared *via* combinatorial mixing of PC and SF solutions followed by evaporation of the solvent at a predetermined rate using the microfluidic chips reported here.

Conclusions

We have developed and validated a hybrid COC-PDMS-thiolene based microfluidic platform for salt screening of PCs at sub-μL scale *via* regulated evaporation of the solvent. The microfluidic platform reported here precisely meters various PC and SF solutions and enables screening of 24 (4 × 6-array) unique combinatorial conditions on-chip by mixing of PC solutions with six different SF solutions *via* FID followed by solvent evaporation at four different predetermined rates. Employment of thin PDMS layers sandwiched between COC sheets (TLA-IL assembly) rendered the chips compatible with solid form analysis *via* Raman spectroscopy as well as with mild organic solvents typically used in pharmaceutical crystallization such as methanol and ethanol, and allowed for long duration crystallization screening experiments (more than 12 h) without significant solvent loss. The solvent-resistant thiolene EL enabled evaporation of the solvent at predetermined rates. The chip requires only ~200 nL of solution for each condition screened, which is two to three orders of magnitude less than the requirements for conventional automated solid form screening platforms (~500 μL per condition). *The small sample size requirement provides an opportunity to initiate solid form screening with more SFs and under more conditions, and thus assessment of the properties of the salts of a PC, at an early stage in the drug discovery and development process, at a time when only limited quantities of each PC (~10 mg) are available*. Therefore, this approach increases the likelihood of identifying a solid form with optimal physicochemical properties for further development. The ease of operation of the microfluidic platform and the requirement of only an external vacuum source for chip operation enable immediate application of these chips in laboratories for solid form screening. Analysis of the resulting solid forms requires additional peripheral equipment, including a bright field microscope to determine size and morphology, crossed polarizers to determine the crystallinity of the solid forms, and a Raman spectroscopy setup for chemical identification. The portability of the chips after completion of the crystallization experiments greatly facilitates analysis of the solid forms, separately from the screening process.

Ephedrine and tamoxifen were used as model compounds to validate the capability of the microfluidic chip to screen and identify multiple salt forms of PCs using only a limited amount of material. Six different salt forms for each of the PCs at different evaporation rates were obtained. Low rates of evaporation led to formation of individual and good quality crystals, whereas high rates of evaporation led to the formation of aggregates of small crystals, gelation, or amorphous precipitation. The identity of the solid forms was confirmed *via* Raman spectroscopic analysis on-chip.

In summary, the platform reported in this paper can be applied to broad screening of suitable salt forms of PCs at different evaporation rates when only limited amounts of each PC are available. One can foresee using this platform for screening other solid forms of PCs (cocrystals and polymorphs) on-chip by inducing controlled supersaturation levels favorable for crystallization *via* solvent evaporation. Previously, we developed chips with different dimensions of the solution chambers that allowed metering of PCs and antisolvents in various volumetric ratios (50 : 10 to 10 : 50), thereby screening different levels of supersaturation on-chip for polymorph screening of PCs.[30] Building on those platforms more comprehensive supersaturation profiles can be screened on-chip, for example by modifying the relative dimensions of the mixing zone and the solution chambers while also integrating evaporation control. The COC/PDMS assembly (TLA-IL assembly) used here should also be compatible with single crystal X-ray analysis and subsequent structure determination of solid forms, as we have recently shown for on-chip protein crystallization.[67] Evaporative crystallization has the capability to allow growth of single, isolated crystals of pharmaceutical solids on-chip, which is very challenging when using other modes of crystallization. Hence, this evaporation based crystallization method can enable on-chip single crystal X-ray analysis for determining the structure and confirm the identity of different solid forms that are hard to distinguish using Raman spectroscopy.

Acknowledgements

We would like to thank AbbVie Inc. for financial support. Part of this work made use of the facilities in the Micro- & Nanotechnology Laboratory as well as the Frederick Seitz Materials Research Laboratory Central Facilities at University of Illinois at Urbana-Champaign, which is partially supported by the U.S. Department of Energy under grants DE-FG02-07ER46453 and DE-FG02-07ER46471. We thank Dr Amit V. Desai and Dr Daria Khvostichenko for stimulating discussions, and Jose Gallegos-Lopez and Araz G. Zarkhah for help in fabrication of the microfluidic platforms.

Notes and references

1 S. L. Morissette, O. Almarsson, M. L. Peterson, J. F. Remenar, M. J. Read, A. V. Lemmo, S. Ellis, M. J. Cima and C. R. Gardner, *Adv. Drug Delivery Rev.*, 2004, **56**, 275–300.
2 E. H. Kerns and L. Di, *Drug Discovery Today*, 2003, **8**, 316–323.
3 L. F. Huang and W. Q. Tong, *Adv. Drug Delivery Rev.*, 2004, **56**, 321–334.
4 C. R. Gardner, C. T. Walsh and O. Almarsson, *Nat. Rev. Drug Discovery*, 2004, **3**, 926–934.
5 M. L. Peterson, M. B. Hickey, M. J. Zaworotko and O. Almarsson, *J. Pharm. Sci.*, 2006, **9**, 317–326.
6 J. Aaltonen, M. Alleso, S. Mirza, V. Koradia, K. C. Gordon and J. Rantanen, *Eur. J. Pharm. Biopharm.*, 2009, **71**, 23–37.
7 C. R. Gardner, O. Almarsson, H. Chen, S. Morissette, M. Peterson, Z. Zhang, S. Wang, A. Lemmo, J. Gonzalez-Zugasti, J. Monagle, J. Marchionna, S. Ellis, C. McNulty, A. Johnson, D. Levinson and M. Cima, *Comput. Chem. Eng.*, 2004, **28**, 943–953.
8 S. M. Berge, L. D. Bighley and D. C. Monkhouse, *J. Pharm. Sci.*, 1977, **66**, 1–19.
9 V. Saxena, R. Panicucci, Y. Joshi and S. Garad, *J. Pharm. Sci.*, 2008, **98**, 1962–1979.
10 A. T. M. Serajuddin, *Adv. Drug Delivery Rev.*, 2007, **59**, 603–616.
11 A. V. Trask, D. A. Haynes, W. D. S. Motherwell and W. Jones, *Chem. Commun.*, 2006, 51–53.
12 J. Zaccaro, J. Matic, A. S. Myerson and B. A. Garetz, *Cryst. Growth Des.*, 2000, **1**, 5–8.
13 S. L. Childs, L. J. Chyall, J. T. Dunlap, D. A. Coates, B. C. Stahly and G. P. Stahly, *Cryst. Growth Des.*, 2004, **4**, 441–449.
14 S. Kim, C. Wei and S. Kiang, *Org. Process Res. Dev.*, 2003, **7**, 997–1001.
15 H. G. Brittain, *J. Pharm. Sci.*, 2010, **101**, 464–484.
16 S. Talreja, M. S., University of Illinois at Urbana-Champaign, 2005.
17 S. Talreja, D. Y. Kim, A. Y. Mirarefi, C. F. Zukoski and P. J. A. Kenis, *J. Appl. Crystallogr.*, 2005, **38**, 988–995.
18 S. Talreja, S. L. Perry, S. Guha, V. Bhamidi, C. F. Zukoski and P. J. A. Kenis, *J. Phys. Chem. B*, 2010, **114**, 4432–4441.
19 S. Talreja, P. J. A. Kenis and C. F. Zukoski, *Langmuir*, 2007, **23**, 4516–4522.
20 G. He, V. Bhamidi, R. B. H. Tan, P. J. A. Kenis and C. F. Zukoski, *Cryst. Growth Des.*, 2006, **6**, 1175–1180.
21 D. L. Chen and R. F. Ismagilov, *Curr. Opin. Chem. Biol.*, 2006, **10**, 226–231.
22 E. D. Carlson, P. Cong, W. H. Chandler, P. J. Desrosiers, C. J. Freitag and J. F. Varni, *United States Pat*, 6939515, 2003.
23 L. Kumar, A. Amin and A. K. Bansal, *Drug Discovery Today*, 2007, **12**, 1046–1053.
24 T. Thorsen, S. J. Maerkl and S. R. Quake, *Science*, 2002, **298**, 580–584.
25 C. L. Hansen, E. Skordalakes, J. M. Berger and S. R. Quake, *Proc. Natl. Acad. Sci. U. S. A.*, 2002, **99**, 16531–16536.
26 R. G. Blazej, P. Kumaresan and R. A. Mathies, *Proc. Natl. Acad. Sci. U. S. A.*, 2006, **103**, 7240–7245.
27 M. R. Thorson, S. Goyal, B. R. Schudel, C. F. Zukoski, G. G. Z. Zhang, Y. Gong and P. J. A. Kenis, *Lab Chip*, 2011, **11**, 3829–3837.
28 B. R. Schudel, C. J. Choi, B. T. Cunningham and P. J. A. Kenis, *Lab Chip*, 2009, **9**, 1676–1680.
29 R. J. Meagher, A. V. Hatch, R. F. Renzi and A. K. Singh, *Lab Chip*, 2008, **8**, 2046–2053.
30 M. R. Thorson, S. Goyal, Y. Gong, G. G. Z. Zhang and P. J. A. Kenis, *CrystEngComm*, 2012, **14**, 2404–2412.
31 B. Zheng, L. S. Roach and R. F. Ismagilov, *J. Am. Chem. Soc.*, 2003, **125**, 11170–11171.
32 P. Laval, J. B. Salmon and M. Joanicot, *J. Cryst. Growth*, 2007, **303**, 622–628.
33 M. Ildefonso, E. Revalor, P. Punniam, J. B. Salmon, N. Candoni and S. Veesler, *J. Cryst. Growth*, 2012, **342**, 9–12.
34 K. Dhouib, C. Khan Malek, W. Pfleging, B. Gauthier-Manuel, R. Duffait, G. Thuillier, R. Ferrigno, L. Jacquamet, J. Ohana, J.-L. Ferrer, A. Theobald-Dietrich, R. Giege, B. Lorber and C. Sauter, *Lab Chip*, 2009, **9**, 1412–1421.
35 G. Kisselman, W. Qiu, V. Romanov, C. M. Thompson, R. Lam, K. P. Battaile, E. F. Pai and N. Y. Chirgadze, *Acta Crystallogr., Sect. A: Found. Crystallogr.*, 2011, **67**, 533–539.
36 Y. Yu, X. Wang, D. Oberthur, A. Meyer, M. Perbandt, L. Duan and Q. Kang, *J. Appl. Crystallogr.*, 2011, **45**, 53–60.
37 A. Y. Lee, I. S. Lee, S. S. Dette, J. Boerner and A. S. Myerson, *J. Am. Chem. Soc.*, 2005, **127**, 14982–14983.
38 L. Li, W. Du and R. F. Ismagilov, *J. Am. Chem. Soc.*, 2009, **132**, 112–119.
39 P. Laval, N. Lisai, J. B. Salmon and M. Joanicot, *Lab Chip*, 2007, **7**, 829–834.
40 D. L. L. Chen, L. Li, S. Reyes, D. N. Adamson and R. F. Ismagilov, *Langmuir*, 2007, **23**, 2255–2260.
41 B. T. C. Lau, C. A. Baitz, X. P. Dong and C. L. Hansen, *J. Am. Chem. Soc.*, 2006, **129**, 454–455.
42 L. Li and R. F. Ismagilov, *Annu. Rev. Biophys.*, 2010, **39**, 139–158.
43 S. L. Perry, G. W. Roberts, J. D. Tice, R. B. Gennis and P. J. A. Kenis, *Cryst. Growth Des.*, 2009, **9**, 2566–2569.
44 M. Ildefonso, E. Revalor, P. Punniam, J. B. Salmon, N. Candoni and S. Veesler, *J. Cryst. Growth*, 2010, **342**, 9–12.
45 J. Shim, G. Cristobal, D. R. Link, T. Thorsen, Y. Jia, K. Piattelli and S. Fraden, *J. Am. Chem. Soc.*, 2007, **129**, 8825–8835.
46 S. Selimovic, F. Gobeaux and S. Fraden, *Lab Chip*, 2010, **10**, 1696–1699.
47 B. Zheng, C. J. Gerdts and R. F. Ismagilov, *Curr. Opin. Struct. Biol.*, 2005, **15**, 548–555.
48 P. Laval, A. Crombez and J.-B. Salmon, *Langmuir*, 2008, **25**, 1836–1841.
49 M. Ildefonso, N. Candoni and S. Veesler, *Cryst. Growth Des.*, 2011, **11**, 1527–1530.
50 J. Shim, G. Cristobal, D. R. Link, T. Thorsen and S. Fraden, *Cryst. Growth Des.*, 2007, **7**, 2192–2194.
51 J. N. Lee, C. Park and G. M. Whitesides, *Anal. Chem.*, 2003, **75**, 6544–6554.
52 S. Goyal, M. R. Thorson, G. G. Z. Zhang, Y. Gong and P. J. A. Kenis, *Cryst. Growth Des.*, 2012, **12**, 6023–6034.
53 H. Christopher, J. T. Cabral, C. M. Stafford, A. Karim and E. J. Amis, *J. Micromech. Microeng.*, 2004, **14**, 153.
54 L. H. Hung, R. Lin and A. P. Lee, *Lab Chip*, 2008, **8**, 983–987.
55 D. Bartolo, G. Degre, P. Nghe and V. Studer, *Lab Chip*, 2008, **8**, 274–279.
56 L.-H. Hung, R. Lin and A. P. Lee, *Lab Chip*, 2008, **8**, 983–987.
57 T. Kojima, S. Onoue, N. Murase, F. Katoh, T. Mano and Y. Matsuda, *Pharm. Res.*, 2006, **23**, 806–812.

58 C. J. Geankoplis, *Transport Processes and Unit Operations*, Prentice Hall, New Jersey, 1993.
59 P. S. Nunes, P. D. Ohlsson, O. Ordeig and J. P. Kutter, *Microfluid. Nanofluid.*, 2010, **9**, 145–161.
60 Z. T. Cygan, J. T. Cabral, K. L. Beers and E. J. Amis, *Langmuir*, 2005, **21**, 3629–3634.
61 M. Allesø, S. Velaga, A. Alhalaweh, C. Cornett, M. A. Rasmussen, F. Van Der Berg, H. L. d. Diego and J. Rantanen, *Anal. Chem.*, 2008, **80**, 7755–7764.
62 F. G. Vogt, J. S. Clawson, M. Strohmeier, A. J. Edwards, T. N. Pham and S. A. Watson, *Cryst. Growth Des.*, 2008, **9**, 921–937.
63 Y. Meng, D. J. Weidner, G. D. Gwanmesia, R. C. Liebermann, M. T. Vaughan, Y. Wang, K. Leinenweber, R. E. Pacalo, A. Yeganeh-Haeri and Y. Zhao, *J. Geophys. Res.*, 1993, **98**, 22199–22207.
64 N. B. Simon, A. C. Edwin, J. D. Roger and J. R. Ron, *J. Pharm. Sci.*, 2007, **96**, 1053–1068.
65 E. A. Collier, R. J. Davey, S. N. Black and R. J. Roberts, *Acta Crystallogr., Sect. B: Struct. Sci.*, 2006, **62**, 498–505.
66 A. McPherson, *Crystallization of Biological Macromolecules*, CSHL press, 1999.
67 S. Guha, S. L. Perry, A. S. Pawate and P. J. A. Kenis, *Sens. Actuators, B*, 2012, **174**, 1–9.